RESEARCH ARTICLE

ADVANCED
ENERGY & SUSTAINABILITY
RESEARCH
Open Access

www.advenergysustres.com

Direct Recycling of β-Li₃PS₄-Based All-Solid-State Li-Ion Batteries: Interactions of Electrode Materials and Electrolyte in a Dissolution-Based Separation Process

Kerstin Wissel,* Aaron Haben, Kathrin Küster, Ulrich Starke, Ralf Kautenburger, Wolfgang Ensinger, and Oliver Clemens

All-solid-state batteries (ASSB) are currently developed at high pace and show a strong potential for market introduction within the next years. Though their performance has improved considerably over the last years, investigation of their sustainability and the development of suitable recycling strategies have received less attention. However, their potential for efficient circular processes must be accessed comprehensively. In this article, the separation of the solid electrolyte β-Li₃PS₄ from different lithium transition metal oxide electrode materials (LiCoO₂, LiMn₂O₄, LiNi₀.₈Mn₀.₁Co₀.₁O₂, LiFePO₄, LiNi₀.₈Co₀.₁₅Al₀.₀₅O₂, and Li₄Ti₅O₁₂) are investigated via an approach based on the dissolution and subsequent precipitation of the thiophosphate using N-methylformamide as solvent. A combination of X-ray diffraction, scanning electron microscopy, energy-dispersive X-ray spectroscopy, inductively coupled plasma mass spectrometry, iodometric titration, and X-ray photoelectron spectroscopy as well as electrochemical impedance spectroscopy and electrochemical characterization is used to characterize the electrolyte and electrode materials before and after separation. Herein, it is found that the presence of electrode materials in the dissolution process can lead to significant chemical reactions. These interactions can (but most not) lead to strong alteration of the electrochemical characteristics of the individual compounds. Thus, it is shown that an efficient recovery of materials likely depends on the precise material combination within an ASSB.

1. Introduction

Since the first commercialization of rechargeable Li-ion batteries (LIBs), this technology has become omnipresent in our everyday lives. In recent years, the exponential growth of consumer electronics and stationary battery markets, coupled with the significant advancement in electronic vehicle technology, has led to a surge in the demand for LIBs—a trend expected to persist in the coming years. However, inherent safety concerns related to the use of combustible liquid electrolytes and limited energy density have also prompted the development of various next-generation battery technologies. Among these, all-solid-state batteries (ASSBs) utilizing solid electrolytes (SEs) are considered highly promising, and different material classes including oxides, polymers, halides, and sulfides are intensively studied with respect to their potential use as SEs.[1] Owing to their high ionic conductivities in the range of 10^{-4}–10^{-2} S cm^{-1}, sulfide-based electrolytes including thiophosphates such as Li–P–S-based glasses or glass ceramics (e.g., xLi₂S•(100 − x)P₂S₅, Li₇P₃S₁₁, β-Li₃PS₄), argyrodites Li₆PS₅X (X = Cl, Br, I), thio-Li super ionic conductors (thio-LISICONs), and Li₁₁₋ₓM₂₋ₓP₁₊ₓS₁₂ (M = Ge, Sn, Si) have gained significant interest.[2]

With the increasing demand for batteries, the development of sustainable recovery and recycling strategies for spent batteries has become a matter of growing urgency. Commonly employed recycling methods for conventional LIBs encompass three types: pyrometallurgical recycling, hydrometallurgical recycling, and direct recycling.[3]

K. Wissel, W. Ensinger
Institute for Materials Science, Materials Analysis
Technical University of Darmstadt
Alarich-Weiss-Straße 2, 64287 Darmstadt, Germany
E-mail: kerstin.wissel@imw.uni-stuttgart.de

The ORCID identification number(s) for the author(s) of this article can be found under https://doi.org/10.1002/aesr.202300280.

K. Wissel, O. Clemens
Institute for Materials Science, Chemical Materials Synthesis
University of Stuttgart
Heisenbergstraße 3, 70569 Stuttgart, Germany

A. Haben, R. Kautenburger
Inorganic Solid State Chemistry
Elemental Analysis
Saarland University
Campus C4 1, 66123 Saarbrücken, Germany

K. Küster, U. Starke
Max Planck Institute for Solid State Research
Heisenbergstraße 1, 70569 Stuttgart, Germany

**ADVANCED
SCIENCE NEWS**

www.advancedsciencenews.com

**ADVANCED
ENERGY & SUSTAINABILITY
RESEARCH**
Open Access

www.advenergysustres.com

Pyrometallurgical recycling entails subjecting the batteries to high-temperature treatments to break down the materials, while hydrometallurgical recycling requires dissolving the battery components to extract metals and other materials individually. The main focus of these recycling strategies employed for LIBs is set on the extraction and recovery of valuable metals such as Li, Co, and other transition metals.[4] Both strategies require energy-intensive resynthesis of each component.[5] Direct recycling, in contrast, involves separation and/or regeneration of battery components without disassembling them into individual constituents to atomic levels. Such nondestructive recycling strategies include, e.g., solid-state calcination, hydrothermal relithiation, eutectic molten-salt relithiation, and dissolution–precipitation processes. Compared to pyrometallurgy and hydrometallurgy, direct recycling approaches are relatively simple, low cost, environmentally friendly, and yield high recovery rates. Therefore, significant research efforts have been made in this field, and various direct regeneration methods for different cathode materials[6] have been proposed.

Although the recycling of LIBs has progressed rapidly, only a limited number of studies have been conducted on ASSBs. With the growing significance of ASSBs, it is crucial to recognize that recycling strategies employed for conventional LIBs may not be directly applicable to ASSBs due to their unique properties, primarily attributed to the chemical nature of the SEs employed in these batteries.[7] With respect to thiophosphate-based ASSBs, pyro- and/or hydrometallurgical recycling processes are not feasible since reactions with water or O_2 lead to a chemical degradation of the electrolyte. In general, the retention of the thiophosphate building units (e.g., ortho-thiophosphate units PS_4^{3-}, meta-thiodiphosphate units $P_2S_6^{2-}$, pyro-thiodiphosphate units $P_2S_7^{4-}$, etc.) during the recycling should be considered key. The economic value of thiophosphates lies not within the contained elements themselves but rather in the P—S bonds which can only be formed from elemental precursors using energy-intensive chemical synthesis approaches.[7a] Related to the potential for solution processing of thiophosphate electrolytes,[8] direct recycling strategies involving the dissolution and subsequent precipitation and recrystallization of the electrolyte might prove to be especially promising.[9] A first proof of principle of this dissolution-based separation strategy has been reported by Tan et al.[10] for a model system of Li|Li₆PS₅Cl|LiCoO₂ employing ethanol as solvent. They were able to separate the insoluble cathode material from the dissolved electrolyte. After the removal of the solvent, Li₆PS₅Cl could be recovered, and the recycled materials could be used to build new batteries.

While Li₆PS₅Cl can be dissolved in ethanol,[11] investigation of the dissolution and recrystallization behavior of β-Li₃PS₄ have shown that ethanol leads to considerable decomposition of the SE, though both electrolytes contain PS_4^{3-} units. For β-Li₃PS₄, we were able to show in a previous study[12] that the polar, weakly protic solvent *N*-methylformamide (NMF) is a suitable solvent allowing for a retention of PS_4^{3-} units during the dissolution and recrystallization. The recrystallization proceeds via an intermediate phase Li₃PS₄ · 2NMF. Thus, depending on the considered thiophosphate SE and the used solvent, complex reactions take place between the electrolyte and the solvent during the dissolution process. The risk for side reactions could increase further due to the presence of different transition metal

oxide (TMO) electrode materials in the dispersion formed after the dissolution of the electrolyte material. Commonly used electrode materials are for example layered materials such as LiCoO₂ (LCO), LiNi₀.₈Mn₀.₁Co₀.₁O₂ (NMC811), LiNi₀.₈Co₀.₁₅Al₀.₀₅O₂ (NCA), spinel-type LiMn₂O₄ (LMO), Li₄Ti₅O₁₂ (LTO), and olivine-type LiFePO₄ (LFP).[13] Thiophosphates are known to have a low electrochemical stability window, which makes them unstable toward charged cathode and anode materials.[14] Already in the discharged state, these TMOs contain transition metal species with oxidation states higher than the preferred oxidation states of stable sulfides.[7a] The presence of dissolved ions such as PS_4^{3-} or S^{2-} might in this context further enhance redox interactions under the formation of metal sulfides, polysulfides, and/or sulfur leading to the degradation of the electrolyte and electrode materials. Other known issues of TMOs[15] like irreversible layer–spinel–rock-salt phase transformation and transition metal ion dissolution might also be influenced and could lower the feasibility of this recycling strategy.

The present study aims to investigate the nature of possible interactions between the dissolved β-Li₃PS₄ and different TMO electrode materials and their influence on functional properties. To relate occurring reactions to a specific electrode material, systematic studies on mixtures of one of the electrode materials and β-Li₃PS₄ are conducted. After a series of different process steps (i.e., dissolution of the electrolyte in NMF, separation of the undissolved electrode material fraction, removal of the solvent and recrystallization of the electrolyte), structural changes of the recycled electrolyte and electrode materials are examined using X-ray diffraction (XRD) and Rietveld analysis. Detailed investigations of morphological and compositional modifications of the electrolyte and electrode fraction are conducted separately. For this, scanning electron microscopy (SEM), energy-dispersive X-Ray spectroscopy (EDX), inductively coupled plasma mass spectrometry (ICP–MS), iodometric titration, and X-ray photoelectron spectroscopy (XPS) are used. Finally, the obtained results are related to the ionic and electronic conductivity of the recycled β-Li₃PS₄ and the electrochemical performance of the recycled electrode materials. This is used to derive information about compatibilities of different components within a solution-based recycling process, and can help to develop direct recycling strategies of thiophosphate-based ASSBs for an establishment of a circular economy of such cells.

2. Experimental Section

2.1. Material Preparation

The pristine electrolyte β-Li₃PS₄ was purchased from NEI Corporation (USA).

The pristine electrode materials LCO, LMO, NMC811, and LTO were synthesized by solid-state reactions using Li₂CO₃ (AlfaAesar, 99%), Co₃O₄ (Thermo Scientific, 99.7%), Mn₂O₃ (Sigma-Aldrich, −325 mesh, 99%), NiO (Sigma-Aldrich, <50 nm, 99.8%), and TiO₂ (Thermo Scientific, anatase, 99.6%, −325 mesh) as precursor materials. Mixtures of stoichiometric amounts of the respective oxides were prepared by intimately grinding using mortar and pestle and heated to 850 °C for 12 h in air, before regrinding and reheating at the same

temperature for further 12 h. The synthesis of $LiNi_{0.8}Co_{0.15}Al_{0.05}O_2$ (NCA) was achieved using a method adopted from Qiu et al.[16] For this, stoichiometric amounts of the metal acetate (hydrate) $Ni(CH_3COO)_2 \cdot 4H_2O$ (Sigma-Aldrich, 99.995%), $Co(CH_3COO)_2$ (Sigma-Aldrich, 99.995%), and $Al(CH_3COO)_2$ (Sigma-Aldrich, basic) were dissolved in deionized water. Excess oxalic acid $C_2H_2O_4$ (Fluka, anhydrous, $\geq$ 99%) was added and the mixture was stirred for 3 h, before drying at 80 °C. The obtained ternary metal oxalate powder was calcined at 450 °C for 6 h in air. $LiOH \cdot H_2O$ (Acros Organics, 98+%) was added in a molar ratio of Li:M = 1.05:1 by thoroughly mixing using mortar and pestle. To obtain the final product, this mixture was heated to 700 °C for 24 h under flowing oxygen. All synthesized electrode materials were directly transferred into an Ar-filled glove box. LFP was purchased from Sigma-Aldrich (>97%, <5 μm particle size).

Further material handling was carried out in Ar atmosphere.

2.2. Separation of β-Li₃PS₄ from Electrode Materials

For the dissolution of β-Li_3PS_4, NMF (99%, Thermo Scientific) was used as solvent. To remove water, it was dried over a molecular sieve (3 Å, 20% m v^{-1}, Sigma-Aldrich). The molecular sieve was removed from the solvent after 72 h via filtration. To avoid any contamination from colloidal molecular sieve particles within the solvent, vacuum distillation was carried out in addition. A residual water content of 20 ppm was determined by Karl Fischer titration (Titrator Compact C10SX, Mettler-Toledo).

Pristine β-Li_3PS_4, one of the pristine active electrode materials, was mixed using mortar and pestle in a 1:1 weight ratio. Subsequently, NMF was added using a solid:liquid ratio of 50 mg:1 mL. After 4 h of stirring, undissolved precipitates were separated from the solution using centrifugation (5000 RPM, 5 min, Hettich Zentrifugen EBA 21). The decanted solution was additionally filtered using a syringe filter (Whatman GD/X 25, pore size: 0.45 μm). Undissolved precipitates were washed three times using additional NMF.

The filtered solution and the washed precipitates were filled into Schlenk flasks which were connected to a Schlenk line. The flask containing the solution was heated to 240 °C under vacuum ($p \approx 5$–8×10^{-2} mbar) for 4 h to remove the excess solvent and to initiate the recrystallization of β-Li_3PS_4. For the precipitates, heating to 120 °C under vacuum was sufficient to remove remaining NMF.

As reference, one experiment was conducted in which only the electrolyte without addition of any electrode material was dissolved; solid:liquid ratio as well as the drying and recrystallization procedure were modified. This sample is referred to as "recrystallized β-Li_3PS_4".

2.3. Characterization

2.3.1. X-Ray Powder Diffraction and Rietveld Analysis

XRD patterns were recorded on a Rigaku SmartLab in Bragg–Brentano geometry with Cu K$_\alpha$ radiation with a wavelength of 1.542 Å and a Hypix-3000 detector. Samples were measured inside low background airtight sample holders (Rigaku), which were sealed inside an Ar-filled glove box.

Analysis of diffraction data was performed via the Rietveld method with the program TOPAS V.6.0. The instrumental intensity distribution of the diffractometer was determined empirically from a fundamental parameter set determined using a reference scan of LaB_6 (NIST 660a). Microstructural parameters (i.e., crystallite size and strain broadening) were refined to adjust the peak shapes.

For the determination of amorphous phase contents, the samples were mixed in a defined weight ratio with Al_2O_3 (calcinated at 1100 °C) and XRD patterns were recorded. The calculation of the respective amorphous fraction was performed using the internal standard method as implemented in TOPAS V.6.0. The phase fraction of unidentified crystalline phase(s) was estimated based on degree of crystallinity determinations also implemented in the software.

2.3.2. SEM and EDX

SEM images were recorded using a secondary electron detector of a Philips XL30-FEG microscope operating at 10 keV. Prior to the measurements, a layer of Au was sputtered onto the samples, which were placed on a carbon pad.

Due to a partial overlap of Au M and S and P K X-ray emission lines, EDX measurements were conducted using an EDAX Genesis detector without an additional coating with gold. For each sample, three spots were measured. Quantitative analysis was performed using the EDAX Genesis software.

2.3.3. ICP–MS

Quantitative elemental analysis of the electrolyte materials via ICP–MS was conducted with an Agilent ICP–MS system 8900 with triple quadrupole ICP–QQQ and SPS4 autosampler. For the sample preparation, $\approx$4 mg of the respective recycled electrolyte material was dissolved in 10 mL ultrapure water (0.055 μS cm^{-2}) (PURELAB Chorus 1 ultrapure water filtration unit, Elga LabWater). A solution with 10 mg l^{-1} of Sc (1 g l^{-1} in 5% nitric acid (HNO₃), Alfa) and Ho (1 g l^{-1} in 2%–3% HNO₃, Merck Certipur) in ultrapure water was prepared as the internal standard stock solution for all ICP–MS measurements. HNO₃ (ROTIPURAN Supra 69%, Carl Roth) was used to acidify the measurement solutions. Argon 5.0 (Ar $\geq$ 99.999 mol%, ALPHAGAZ 1 Argon, Air Liquide) was used as plasma gas for ICP–MS measurements. For calibration purpose Li (1 g l^{-1} in 0.5 M HNO₃, Merck Certipur), Al (1 g l^{-1} in 0.5 M HNO₃, Bernd Kraft), P (1 g l^{-1} in water, AccuStandard AccuTrace), Ti (1 g l^{-1} in water with a trace of hydrofluoric acid, VWR International), M (1 g l^{-1} in 0.5 M HNO₃, Fluka), Fe (1 g l^{-1} in 0.5 M HNO₃, Merck Certipur), Co (1 g l^{-1} in 0.005 M HNO₃, Fluka), and Ni (1 g l^{-1} in 0.005 M HNO₃, Fluka) ICP–MS standards solutions were used. The measurements were performed with different reaction cell gas modes: ^{31}P was measured in O_2 reaction gas mode via mass pair $(Q_1, Q_2) = (31, 47)$, ^{27}Al, ^{47}Ti, ^{55}Mn, ^{56}Fe, ^{59}Co, and ^{60}Ni in He collision gas mode and ^7Li in "NoGas"-mode. An external calibration was done for quantification.

ADVANCED
SCIENCE NEWS
www.advancedsciencenews.com

ADVANCED
ENERGY & SUSTAINABILITY
RESEARCH
Open Access
www.advenergysustres.com

2.3.4. Electrochemical Impedance Spectroscopy

Electrochemical impedance spectroscopy (EIS) of the pristine as well as of the recycled electrolyte materials after separation from the electrode materials was performed using a TSC battery test cell (rhd instruments GmbH & Co. KG). Heating and cooling were achieved with a temperature-controlled cell stand. For this, 30 mg of each powder was uniaxially pressed into a free-standing pellet with a diameter of 7 mm (pelletizing pressure of 254 MPa for 5 min). The thickness of the obtained pellets was measured using calipers. Gold layers were sputter-coated onto the surfaces. Electrical impedance measurements were performed using an electrochemical impedance analyzer NEISYS (Novocontrol Technologies) in a frequency range between 1 MHz and 0.1 Hz with a root-mean-square amplitude of 10 mV in a temperature range between 20 and 80 °C ($\Delta T = 5$ K, heating and cooling). Received data was analyzed using the software RelaxIS3 (rhd instruments GmbH & Co. KG).

2.3.5. Chronoamperometry

For chronoamperometry (CA) measurements pellets of the electrolyte materials with blocking gold electrodes were prepared as described earlier. A constant potential of 2 V was applied and the current–time response was recorded over a duration of 12 h to obtain a steady-state current measurement. The measurements were performed with a VMP potentiostat (BioLogic Science Instruments).

2.3.6. Iodometric Titration

For iodometric titration experiments, ≈30 mg of a respective electrode material was dissolved in a mixture of 15 mL 20% KI solution and 15 mL 1 M HCl. The KI solution and HCl were freshly prepared using Ar-flushed water. Back titration was carried out using a 5 mM $Na_2S_2O_3$ solution, and 5–8 drops of 1 wt% starch solution were added as indicator. To minimize atmospheric oxidation, the experiments were performed under a flow of Ar.

2.3.7. X-Ray Photoelectron Spectroscopy

For the preparation of XPS samples, double-sided adhesive tape, functioning in addition as an insulating layer, was used. Small quantity of powders of selected electrode materials was placed unto the tape which was previously stuck to the sample holder. Samples were transferred under Ar into the XPS chamber.

The X-ray photoelectron data were recorded using a Kratos AXIS Ultra spectrometer and monochromatized Al Kα radiation. Survey spectra were acquired with a pass energy of 80 eV and detailed spectra with a pass energy of 20 eV. A charge neutralizer was used to compensate for the surface charging.

The binding energies were calibrated to the C—C peak of adventitious carbon in the C 1s spectrum at 284.8 eV.[17] Data analysis was performed using the CasaXPS software.[18] To determine the integral intensity of the emission lines, the spectra were background-corrected according to Shirley.[19] For the fitting of the spin−orbit split of the S $2p_{3/2}$ and S $2p_{1/2}$ peaks, the binding energy separation was set to 1.18 eV[20] and the area ratios were constrained to 2:1.

2.3.8. Electrochemical Testing

For electrode preparation, 85 wt% of pristine and recycled active electrode materials were mixed homogeneously with 5 wt% carbon black Super P (TIMCAL Ltd., Switzerland) as conducting additive and 10 wt% polyvinylidene fluoride (Solef PVDF, Solvay, Germany). The binder solution consisted of 10 wt% PVDF in N-methyl-2-pyrolidone (BASF, Germany). The obtained slurries were tape-casted onto aluminum or copper foils. After tape-casting, the printed electrodes were dried at 55 °C for 24 h. Round electrodes with a diameter of 7.8 mm were cut out and the weight of the electrodes was measured. The electrodes were dried under vacuum in a Büchi oven (Büchi glass oven B-585) at 80 °C for 24 h before being transferred without further contact with air into an argon-filled glove box for cell assembly.

For testing, cells of two-electrode Swagelok-type setup were assembled. Reference/counter electrodes with a diameter of 8 mm were stamped out of Li foil (thickness 0.75 mm, diameter 5 mm, Sigma Aldrich). Glass fiber membranes (Whatman GF/C) were used as separator, which were soaked in 180 µL electrolyte. As electrolyte a solution of 1 M LiPF$_6$ in ethylene carbonate: dimethyl carbonate, ratio 1:1 (LP30, Merck KGaA, Germany), was used. The testing was performed with a VMP potentiostat (BioLogic Science Instruments). Cyclic voltammetry (CV) measurements were conducted in suitable potential ranges for the respective active electrode with a scan rate of 0.1 mV s^{-1}. Galvanostatic charging with potential limitation (GCPL) was performed using different C rates of C/10, C/5, C/2, C, and 2C (five cycles for each C rate) with charging/discharging currents calculated in relation to the active electrode mass excluding the mass of the carbon black and PVDF used in electrode preparation. The different constant currents were applied to evaluate the cycling stability and the rate performance.

3. Results and Discussions

After the separation of the dissolved Li_3PS_4 and the electrode materials (investigated electrode materials are LCO, LMO, NMC811, LFP, NCA, and LTO), both fractions were dried under vacuum to remove the solvent NMF. To obtain a recrystallization of the electrolyte to β-Li_3PS_4, heating parameter were chosen according to our previous findings on the recrystallization behavior of β-Li_3PS_4.[12]

First indications for different reactivities between the electrode materials and the dissolved electrolyte can be observed when comparing the colors of the solutions after the separation of the electrodes (Figure S1, Supporting Information). The strongest color changes are found for the solution separated from LFP (dark greenish-brown color) and NCA (dark yellow). In contrast to this, the solution separated from LTO remains colorless. Such changes could be related to formation of polysulfides Li_2S_x and, thus, decomposition of ortho-thiophosphate units PS_4^{3-} might be indicated. Dissolved polysulfides are known to have a very complex influence on the color of solutions with a strong dependence on the value of $\times$ and the concentration of such species.[21]

ADVANCED
SCIENCE NEWS

www.advancedsciencenews.com

ADVANCED
ENERGY & SUSTAINABILITY
RESEARCH
Open Access

www.advenergysustres.com

In addition, it should be noted that transition metal complexes can also affect the color of a solution significantly.[22] Even though, there are many factors (e.g., type of transition metal and ligand, as well as coordination numbers, geometries, and symmetries of the transition metal complex) influencing the color, this points to a certain solubility of the transition metals from the electrode materials.

After the removal of the solvent, all recycled electrolyte and electrode materials are optically indistinguishable compared to their pristine counterparts. The only exception is found for LFP for which a color change from grey for the pristine LFP to black for the recycled LFP is observed (Figure S2, Supporting Information). This points already to compositional changes due to interactions with the dissolved Li_3PS_4 and/or dissolution of LFP.

3.1. XRD Study

To receive insights into possibly occurring interactions between the dissolved Li_3PS_4 and the electrode materials, an XRD study was performed. Comparing the diffraction patterns of the recycled electrolytes and electrode materials received after drying (and recrystallization) to the pristine materials, significant differences can be found (**Figure 1**). Quantitative phase analysis was conducted using the Rietveld method (see Table S1 and S2, Supporting Information, for quantitative analysis and refined lattice parameters).

For the recrystallized and recycled electrolyte powders (Figure 1a), the main phase observed after the separation procedure is β-Li_3PS_4. Compared to the pristine β-Li_3PS_4, a small contraction in the a lattice parameters (<1%) are found. At the same time, the b lattice parameters increase in the same order of magnitude, resulting in overall comparable unit cell volumes between

≈ 641 and 645 Å^3. Similar trends have been observed for nanoporous β-Li_3PS_4 (synthesized from the Li_3PS_4·3THF complex through annealing at $160\,°C$) upon heating to higher temperatures than needed for the synthesis and can be likely related to a gradual release of residual solvent or solvent decomposition products.[23]

Furthermore, additional reflections of unidentified phase(s) are found in all recycled electrolytes except for the electrolyte separated from LMO. Within the crystalline phase fraction, these phases account for up to ≈ 12 wt% with the highest weight fraction found for the electrolyte separated from NCA; LCO, NMC811, LFP, and LTO contain between ≈ 5 and 7 wt% of these phases. Since the intensity ratios of these additional reflections differ from sample to sample, it is indicated that several impurity phases are formed. The formation of other thiophosphates with other thiophosphate units (e.g., $Li_2P_2S_6$, $Li_7P_3S_{11}$, or $Li_4P_2S_6$)[24] is not observed. Additionally, the impurity phase Li_2S found in pristine β-Li_3PS_4 (≈ 3 wt%) is not found in the recycled materials indicating that it is, e.g., consumed due to reactions with the electrode materials during the dissolution process and/or increases the Li and S contents in the amorphous matrix of the electrolyte fraction (possible also enabling the formation of the unidentified crystalline phases(s) after recrystallization).

In general, a considerable increase of the amorphous phase fractions from $\approx 8\%$ in the pristine β-Li_3PS_4, to $\approx 35\%$ in the recrystallized β-Li_3PS_4 and to ≈ 37–56% in the recycled β-Li_3PS_4 are observed suggesting a dependence of the recrystallization behavior of recycled β-Li_3PS_4 on the electrode material the electrolyte was separated from (e.g., due to the partial dissolution of the electrode materials). For the recycled electrolytes, the lowest increase in amorphous phase fraction was observed for the electrolyte separated from LTO; the highest amorphization is found for LMO, LFP, and NCA. Interestingly, for the
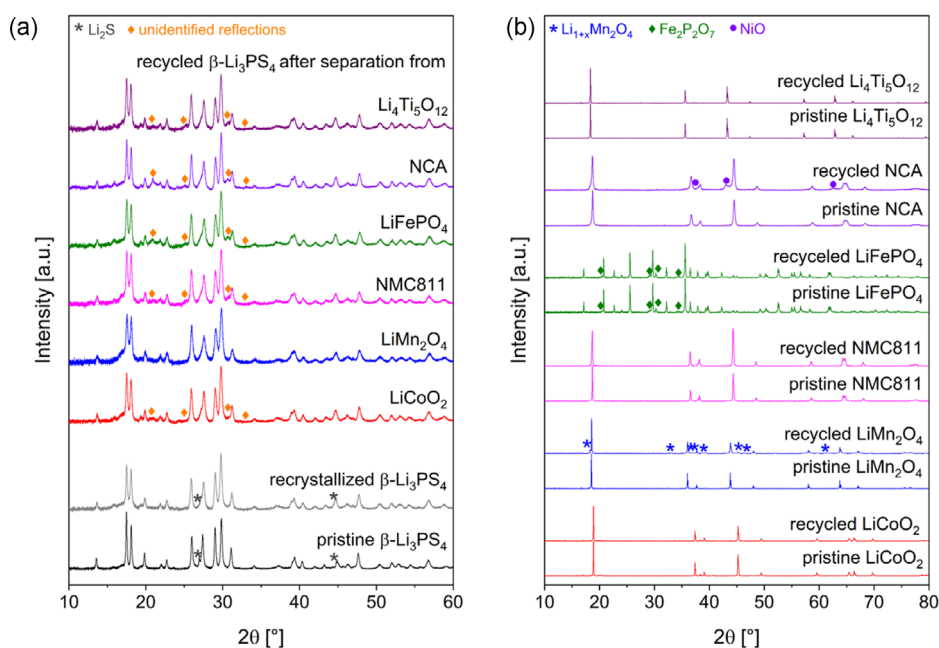

Figure 1. XRD patterns a) of recycled β-Li_3PS_4 after separation from different electrode materials and b) of recycled electrode materials in comparison to the respective pristine materials.

**ADVANCED
SCIENCE NEWS**

www.advancedsciencenews.com

**ADVANCED
ENERGY & SUSTAINABILITY
RESEARCH**
Open Access

www.advenergysustres.com

electrolyte separated from LMO, a strong amorphization takes place, while no unidentified crystalline phases are formed. This might suggest different degradation reactions compared to the other electrolyte materials.

These observed changes can be partially related to the differences observed between the pristine and recycled electrode materials (Figure 1b). While the XRD patterns of LCO, NMC811, LFP (phase fractions of impurity phase remain fairly constant in pristine and recycled LFP), and LTO are unchanged; additional crystalline phases can be found in the recycled LMO and NCA. Interestingly, the formation of crystalline transition metal sulfides is not observed in any of the XRD measurements. It should be noted that quantification errors in Rietveld analysis are in the order of 1–2 wt%. Thus, phase fractions of other crystalline phases might be too low to be detected (e.g., formation of a layer of metal sulfides on the surface of the electrode material particles).

In the case of the recycled LMO, ≈ 17 wt% of $Li_{1+x}Mn_2O_4$ ($x \leq 1$) are present besides $LiMn_2O_4$. This suggests that $LiMn_2O_4$ can be further lithiated due to the presence of Li^+ and S^{2-} ions in solution (the latter acts as reductant). This leads, however, to a Li deficiency in the electrolyte fraction after separation. This implies that P- and S-rich phases might be formed, which could account to the high amorphous phase fraction of the recycled electrolyte. The absence of such Li-rich phases might also suggest that the unidentified crystalline phase(s) found in the electrolytes separated from other electrodes might be Li richer. The lithiation of the electrode material is correlated to an oxidation state change of the transition metal ion Mn from +III/IV in $LiMn_2O_4$ to +III in $Li_2Mn_2O_4$. The spinel-type $LiMn_2O_4$ represents a semi-discharged state of lithium manganese oxide cathode materials, while $Li_2Mn_2O_4$ can be considered fully discharged. Thus, such interactions can result in significant changes and degradation of both the electrolyte and the electrode material.

For recycled NCA, another degradation mechanism under the formation of ≈ 17 wt% NiO-like rock-salt phase is observed. Such instabilities can be related to the reduction tendency of Ni^{3+} to Ni^{2+} in Ni-rich cathodes (compare also degradation in ambient air).[25] The formation of NiO is only possible considering significant structural transformations of the electrode material connected to the inherent structural instability of layered oxides. This has been also observed in the context of cation-mixing which results in a gradual transformation of the layered structure into a spinel-like structure and finally into the rock-salt phase. This takes typically place starting on the surface and gradually permeates into the bulk.[26] The presence of PS_4^{3-} and/or S^{2-} in the solution might accelerate this degradation process. In particular, sulfide ions might lead to the stabilization of the preferred stable +II oxidation state of Ni under the formation of NiS. Reactions between NCA and the dissolved electrolyte would also imply that the recycled electrolyte would undergo a certain degradation due to a partial transformation of Li—P—S bonds into Li—P—O bonds. Such phases might contribute to the high amorphous phase fraction found in the recycled electrolyte separated from NCA. A similar behavior could be expected for NMC811 since it is also Ni rich. Interestingly, the formation of crystalline NiO was not observed for the recycled NMC811. This could be correlated to the different particle sizes and surface areas of NMC811 and NCA (see also Section 3.3).

3.2. Detailed Investigation of Electrolytes

As was described in Section 3.1, interactions between the dissolved electrolyte and the electrode materials do not only result in the formation of crystalline phases but also lead to significant amorphization. Thus, the identification of changes based on XRD alone can be difficult. Special attention has to be given to the amorphous phase fractions present in the samples which increase considerably compared to pristine β-Li_3PS_4. Due consideration has to be given to other occurring morphological and compositional changes since these can significantly impact the functional properties of the recycled β-Li_3PS_4. Therefore, additional studies on such changes are required to find correlations to the ionic and electronic conductivities of the recycled electrolytes. With respect to ionic conductivity, it has been shown that higher crystallinity in Li_3PS_4 does not necessarily lead to improved properties[27]; however, even subtle changes in the chemical composition can affect structural and correlated transport properties significantly. Investigating the detailed composition might allow to draw conclusions on influencing factors.

To investigate morphology changes between the pristine and recycled β-Li_3PS_4 after separation from different electrode materials, SE micrographs were recorded (**Figure 2**). In agreement with our previous study on the recrystallization of β-Li_3PS_4 from NMF,[12] the morphologies of pristine and recycled β-Li_3PS_4 differ significantly. Compared to pristine β-Li_3PS_4, the recycled β-Li_3PS_4 powders consist of irregularly shaped particles with a wider particle size distribution. A higher fraction of smaller particles is observed. The larger particles in the recycled electrolytes appear to be flake-like and splintery. Closest resemblance might be found between the pristine β-Li_3PS_4 and recycled β-Li_3PS_4 separated from LTO. Such changed particle shapes and, in particular, smaller particle sizes could considerably influence the ionic conductivity of the recycled β-Li_3PS_4.

Composition changes within the recycled electrolytes due to a possible transfer of transition metals related to undesired dissolution of the electrode materials were examined using ICP–MS measurements (EDX could not give meaningful insights due to the relatively high limit of detection of this method not suitable for trace analytes). A partial dissolution of transition metal ions could have significant impact not only on the electrode material itself, but also on the electrolyte fraction. Here, a dependence on the concentration of the transition metal, the type of phase formed incorporating the transition metal and its properties, as well as the distribution of this phase within the electrolyte phase can be expected. Furthermore, with respect to amorphous phase fractions, which can significantly influence the transport properties of thiosulfate electrolytes,[27] two aspects have to be considered: 1) the recrystallization behavior of β-Li_3PS_4 after its dissolution could be considerably changed due the presence of transition metal ions in the solution; 2) the formations of the phase containing the transition metal might possibly result in elemental deficiencies within the electrolyte fraction with formal composition of Li:P:S of 3:1:4, hindering the formation of crystalline β-Li_3PS_4 and affecting the short-range order.
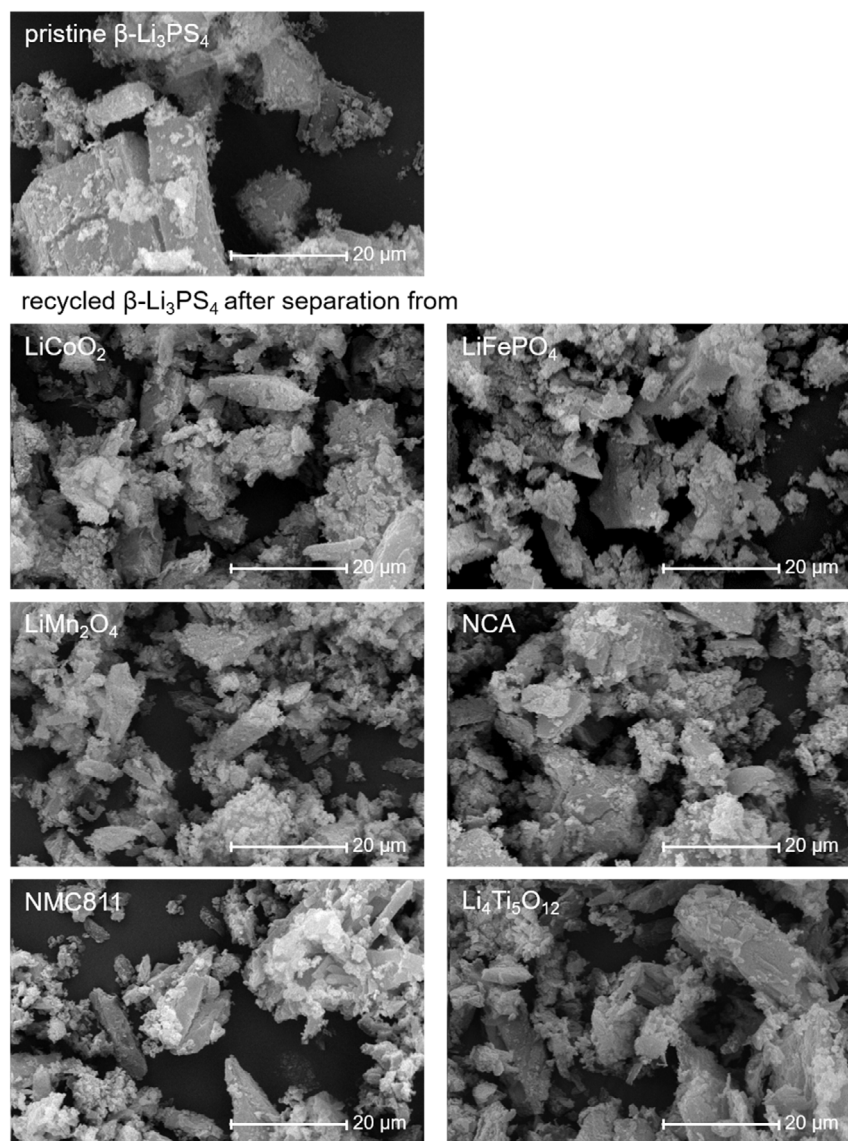
Figure 2. SE micrographs of pristine and recycled β-Li$_3$PS$_4$ after separation from different electrode materials.

The molar ratios of Li, Al, Ti, Mn, Fe, Co, and Ni to P based on ICP–MS measurements are summarized in **Table 1** (molar concentrations are provided in Table S3, Supporting Information). Owing to problems with the precise quantification of sulfur, no sulfur concentrations are reported. The Li:P molar ratio is in all materials close to 3 and comparable values between the pristine and recycled electrolytes are found. Slight deviations might relate to Li (or P) transfer between the electrode and electrolyte materials. Compared to the pristine β-Li$_3$PS$_4$, increased concentrations of Mn, Co, and Ni can be observed in the recycled electrolytes though overall comparatively low elemental transfer is found. The highest increase in concentration is found for Mn in the electrolyte separated from LMO. With respect to this dissolution, the formation of NMF-soluble MnS under the stabilization of Mn^{2+} might play a role. For the electrolytes separated from NMC811 and NCA, increases in the Ni concentrations are observed; again,

stronger reactivities are found for the electrolyte separated from NCA. The concentrations of the Mn and Co are similar to what is found in pristine β-Li$_3$PS$_4$. It should be noted that the concentrations of Al and Fe are below the limits of quantifications (marked with ND–"not determined"); the only exception is found for β-Li$_3$PS$_4$ separated from LFP showing increased Fe concentrations. Low Ti concentrations in the electrolyte separated from LTO point to the high stability of LTO during the dissolution and separation process.

The compositional changes within the recycled electrode materials can be also related to the observed increase of the amorphous phase fraction of the recycled electrolytes. The partial dissolution of transition metals and subsequent incorporation into the electrolyte after solvent removal leads to an altered defect chemistry of the material, which can well explain the increased amount of amorphous phase. In addition, the impact of the

Table 1. Molar ratios of Li, Al, Ti, Mn, Fe, Co, and Ni to P of pristine and recycled β-Li$_3$PS$_4$ after separation from different electrode materials based on quantitative ICP–MS analyses. S contents were not determined.

				Molar ratio			
–	Li:P	Al:P	Ti:P	Mn:P	Fe:P	Co:P	Ni:P
Pristine β-Li$_3$PS$_4$	3.09	ND	5.15×10^{-5}	1.76×10^{-5}	ND	1.01×10^{-6}	2.74×10^{-5}
β-Li$_3$PS$_4$ separated from							
LiCoO$_2$	3.14	ND	2.89×10^{-5}	7.66×10^{-6}	ND	3.00×10^{-6}	ND
LiMn$_2$O$_4$	3.03	ND	3.24×10^{-5}	1.35×10^{-3}	ND	1.23×10^{-7}	8.50×10^{-6}
NMC811	3.22	ND	1.98×10^{-5}	3.92×10^{-5}	ND	4.98×10^{-7}	6.89×10^{-5}
LiFePO$_4$	3.03	ND	2.68×10^{-5}	1.38×10^{-5}	6.61×10^{-4}	3.41×10^{-7}	1.58×10^{-5}
NCA	3.09	ND	1.62×10^{-5}	2.67×10^{-5}	ND	7.45×10^{-6}	5.14×10^{-4}
Li$_4$Ti$_5$O$_{12}$	3.10	ND	3.54×10^{-5}	1.18×10^{-5}	ND	9.02×10^{-8}	ND

transition metals on the thiophosphate groups leading to the formation of, e.g., polysulfides or P—O bonds could induce additional defects in the electrolyte and lower the degree of crystallinity further.

As already noted, these morphological and compositional changes can be expected to have an influence on the functional properties (e.g., ionic and electronic conductivity) of the recycled electrolyte materials. Therefore, EIS and CA measurements were performed. The Nyquist plots of pristine, recrystallized, and recycled β-Li$_3$PS$_4$ are separated from the different electrode materials (measured at 25 °C), as shown in **Figure 3**a. It was found that one parallel R/CPE element (R = resistor, CPE = constant phase element) connected in series to a CPE can be used for fitting the Li-ion transport process and the electrode-ion-blocking effect at the electrode; for recycled β-Li$_3$PS$_4$ separated from NCA, a model with two parallel R/CPE elements in series to a CPE is required (see also Figure S4, Supporting Information). From the fits, the RT conductivity values and activation energies were determined (Figure 3b); the Arrhenius plots are provided in Figure S3a, Supporting Information. The Nyquist and Bode (see also Figure S4, Supporting Information) plots of all samples are fairly similar with the exception of β-Li$_3$PS$_4$ separated from NCA and LFP. This shows that the formation of impurity phases, the increase of amorphous phase fractions as well as the partial

dissolution of transition metal ions do not necessarily lead to a significant change of the impedance response (depending on the overall amounts of these phases). The RT ionic conductivities are in the same order of magnitude after the separation except for LFP and NCA (see Figure 3b). The activation energies of the recrystallized and recycled electrolyte materials are comparable to those of other β-Li$_3$PS$_4$ synthesized via solvent-based preparation approaches.[21,28,29]

In contrast, the sample separated from LFP shows a considerable increase of the resistance, while the activation energy decreases significantly suggesting considerable modification of the Li-ion transport properties due to the observed interactions between the electrolyte and electrode material. For β-Li$_3$PS$_4$ separated from NCA, a significantly different frequency dependence of the impedance and phase angle (compare also Figure S3b and S4, Supporting Information) and a strong decrease of the conductivity is observed. For both samples, the increasing resistances can be in principle correlated to the powder diffraction analysis which reveals not only the increased formation of amorphous phases compared to other electrode materials, but also the presence of a comparatively large phase fraction of the presumably more resistive, unidentified phase(s). The strong interreactivity of dissolved Li$_3$PS$_4$ and these samples is also indicated by strong color change of the Li$_3$PS$_4$ containing NMF solution
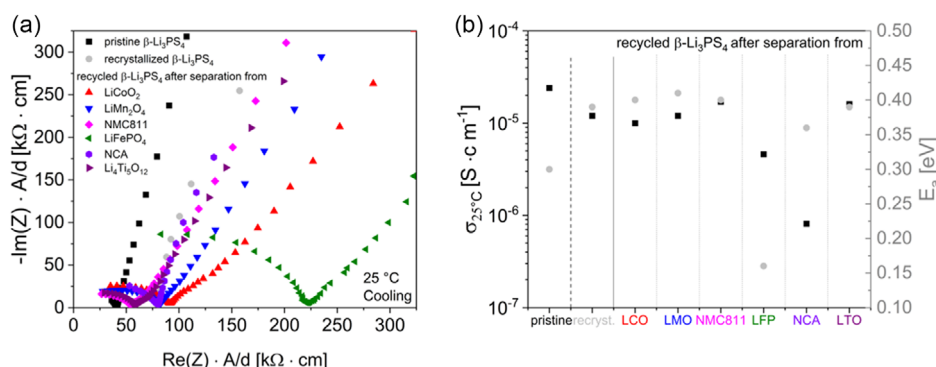

Figure 3. a) Nyquist plots of pristine, recrystallized and recycled β-Li$_3$PS$_4$ after separation from different electrode materials measured at 25 °C. The extended spectrum of recycled β-Li$_3$PS$_4$ after separation from NCA is given in Figure S3, Supporting Information; b) ionic conductivities $\sigma_{25\,°C}$ and activation energies E_a of pristine, recrystallized and recycled β-Li$_3$PS$_4$ after separation from different electrode materials.

**ADVANCED
SCIENCE NEWS**

www.advancedsciencenews.com

**ADVANCED
ENERGY & SUSTAINABILITY
RESEARCH**
Open Access

www.advenergysustres.com

obtained after separation from LFP as well as of recycled LFP and the strong degradation of NCA under the formation of NiO, respectively. In addition, different elemental impurities are indicated in both samples. Further, LFP and NCA show a very different redox behavior after separation (see Section 3.3).

Remarkably, it should be emphasized that the observed distinct redox reaction between LMO and β-Li$_3$PS$_4$ does not result in a significant impact on the conductivity. This indicates that side reactions are complex. The detailed nature of additional phases formed depends strongly on the electrode material, and the interactions can affect the conductivity to different extents. Further detailed analyses are required to deconvolute all possible influence factors and assign their individual impact on the overall conductivity.

The electronic conductivity of the recycled β-Li$_3$PS$_4$ was measured to be between $\approx 7.8 \times 10^{-10}$ and 1.3×10^{-9} S cm^{-1} by CA (Figure S5, Supporting Information). The pristine and recrystallized β-Li$_3$PS$_4$ have comparable electronic conductivities of $\approx 9.7 \times 10^{-10}$ and 4.9×10^{-10} S cm^{-1}, respectively. These values are consistent with previously reported electronic conductivities for thiophosphate SEs,[30] and the electronic contribution to the total conductivity is negligibly low.[31] Thus, the separation process does not lead to an increased electronic conductivity.

3.3. Detailed Investigation of Electrode Materials

Similar to the recycled electrolytes, morphological and composition changes can have significant influence on electrochemical properties of the recycled electrode materials. Due to the comparably low solubility of the investigated electrode materials, reactions are very likely to predominantly take place between the electrolyte ions in solution and the particle surfaces of the electrode materials, potentially leading to the formation of interfacial reaction products. Reactions occurring on the electrode material particle surfaces play a significant role since they can lead to the formation of beneficial protective layers on the particles. For example, modifications of electrode materials using sulfur, polysulfides, or Li$_2$S additives have been shown to improve the electrochemical performance due to the formation of artificial cathode electrolyte interphases.[32] However, it might also be possible that unfavorable passivating layers are formed. Even though initial findings on compositional changes could be made based on XRD, detailed investigations on, e.g., oxidation state and overall composition changes are required.

The morphology of the pristine and recycled electrode materials was examined using SE microscopy (**Figure 4**). The shape and the size of the particles of the pristine electrode materials correspond to accordingly synthesized materials reported in literature[16,33] Compared to the materials prepared via solid-state reactions, significantly smaller particle sizes are found for NCA synthesized using a wet-chemical approach. All materials show particle agglomeration. No difference between the pristine and recycled materials is observed indicating that the electrode materials remain relatively unchanged in terms of morphology.

For the determination of the chemical composition of the pristine and recycled electrode materials, EDX measurements were performed (Table S4, Supporting Information). Within the error of this technique, the compositions of the electrode materials could be confirmed (in agreement with additional ICP–MS measurements). For the recycled electrode materials, additional signals corresponding to P and S are found, pointing toward carryover of these elements (presumably primarily on the particle surfaces) into the electrode material fraction after the separation. For recycled LCO, LMO, NMC811 (one deviating measurement might indicate compositional inhomogeneities), and LTO, these signals account for <1 at% of P and S. Recycled NCA shows higher amounts of P and S with up to $\approx$2 at% of P and $\approx$4 at% of S. For recycled LFP, overall lower P contents compared to the pristine materials might suggest a partial transfer of P (or PO$_4^{3-}$ units) into the solution and with this into the electrolyte fraction; S amounts are comparable to the values observed for recycled LCO, LMO, NMC811, and LTO.

XRD of the recycled electrode materials (Section 3.1) reveals the formation of crystalline Li$_{1+x}$Mn$_2$O$_4$ (also in agreement with ICP–MS results indicating an increase of Li content in the recycled LMO, see Table S4, Supporting Information) and
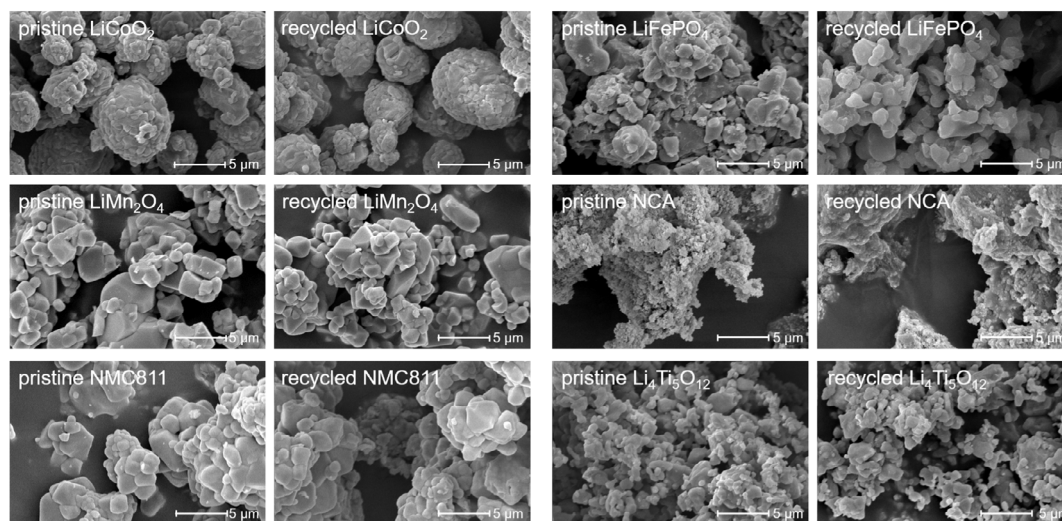

Figure 4. SE micrographs of pristine and recycled electrode materials.

NiO in the case of recycled LMO and NCA, respectively. Relatable changes of the average oxidation states of the transition metal cations of the electrode materials were determined using iodometric titration (**Table 2**). For LMO and NCA, lowered oxidation states compared to the pristine materials are observed, which correspond well to the expected degree of lowering with respect to the quantitative Rietveld analysis and the determined compositions. All other electrode materials possess average oxidation states close to the ideal oxidation states expected based on their composition. The oxidation state of LTO could not be determined due to its low solubility; its white color indicates, however, the presence of Ti^{4+}.[34]

To qualitatively investigate differences of surface compositions of the electrode materials before and after the dissolution-based separation process, XPS measurements were performed. As shown earlier, the strongest interactions between dissolved β-Li_3PS_4 and the electrode materials were found for the electrolyte fractions separated from LFP and NCA and/or the electrode materials LMO, LFP, and NCA. Therefore, in the following, a focus is set on the investigation of these electrode materials. The 2p XP spectra of the respective main transition metal (Mn 2p for LMO, Fe 2p for LFP, and Ni 2p for NCA) as well as the P 2p and of S 2p spectra are given in **Figure 5**. Additional spectra (e.g., O 1s and C1s) are provided in Figure S6, Supporting Information. Interestingly, though the measurement parameters were identical, a comparison between the spectra of the main transition metals of the pristine and recycled electrode materials reveals significant differences in terms of counts per seconds (please consider the different scaling of the y axis of the pristine and recycled spectra), which is especially pronounced for LFP and NCA. This might indicate that the surfaces of the recycled LFP and NCA particles have a Fe and Ni deficiency due to the presence of P- and/or S-rich surface contaminations, respectively. In contrast to this, the intensities of the Mn 2p spectra of pristine and recycled LMO are comparable.

For LMO, the comparison between the Mn 2p spectra of the pristine and recycled electrode material (Figure 5a) shows a

Table 2. Comparison of ideal and measured average oxidation states of the transition metal(s) (TM(s)) of pristine and recycled electrode materials determined by iodometric titration. *For $LiFePO_4$, no significant color change of the solution after addition of KI and/or starch solution was observed, indicating a Fe oxidation state very close to +2.

	Ideal average oxidation state of TM [s]	determined average oxidation state of TM [s]
Pristine $LiCoO_2$	3	2.89
Recycled $LiCoO_2$		2.87
Pristine $LiMn_2O_4$	3.5	3.43
Recycled $LiMn_2O_4$		3.36
Pristine NMC811	3	2.81
Recycled NMC811		2.78
Pristine $LiFePO_4$	2	2.05*
Recycled $LiFePO_4$		2*
Pristine NCA	3	3.02
Recycled NCA		2.73

significant shift of the Mn $2p_{3/2}$ and $2p_{1/2}$ signals toward lower binding energies, indicated by the shift of the center of gravity of the signals. The exact quantification of the oxidation state of Mn based on the Mn 2p spectrum is complicated due to the close proximity of Mn^{4+}, Mn^{3+} and Mn^{2+} emission lines and their multiple splitting.[35] However, the position of the Mn $2p_{3/2}$ between $\approx$ 640 and 644 eV indicates a mixture of Mn in +2, +3, and +4 oxidation states. This result is in good agreement with our previous findings since the observed lithiation of $LiMn_2O_4$ to $Li_{1+x}Mn_2O_4$ leads to a lowering of the overall oxidation state toward +3. In addition, the increase of the intensity of the shoulder at $\approx$640.9 eV in the recycled LMO suggests an increased contribution of Mn^{2+}.[36] This lower surface oxidation state might be related to the formation of MnS on the particle surfaces, reported at binding energies of 640.9 eV.[37]

The P 2p spectra of the pristine and recycled LMO differ significantly. While no P-containing species are found on the pristine material, a P 2p signal is found in the recycled LMO. The binding energy of the main signal of P—S bonds in the PS_4^{3-} units of β-Li_3PS_4, which could be expected to be present on the particles after the separation process, is reported to be at 132.0 eV.[38] However, the center of gravity of the P 2p signal is shifted toward higher binding energies suggesting a considerable formation of, e.g., P—$[S]_n$—P as well as oxygenated phosphorous species (phosphates, metaphosphates or $PS_{4-x}O_x^{3-}$).[39]

The formation of sulfidic species on the surfaces of recycled LMO is indicated based on the S 2p spectrum. Fitting of the spectrum (fit not shown, see also shoulder at $\approx$164.3 eV) suggests that at least two different doublet contributions at energies of $\approx$161.7 and 162.9 eV and of $\approx$163.1 and 164.3 eV, respectively, are required. An unambiguous assignment of the signals found at lower binding energies is not possible since different sulfidic species such as, MnS (reported $2p_{3/2}$ binding energies between 161.4 and 162 eV)[40] and MnS_2 (reported $2p_{3/2}$ binding energy $\approx$161.9),[41] but also Li_3PS_4[38,42] could be present impeding the deconvolution; the doublet signal at higher binding energies can be assigned to P—$[S]_n$—P species.[43] It should be noted that the spectrum of pristine LMO features a signal at binding energies characteristic for metal sulfates.[44] This might be related to reactions between the freshly synthesized LMO and gaseous sulfur species after the transfer into the glove box in which numerous sulfur-containing compounds are stored. After the separation process, these metal sulfates are not present on the recycled materials particles.

For LFP and NCA, similar observations can be made in general. The comparison between the Fe 2p spectra of the pristine and recycled LFP shows, however, in agreement with the previous results no significant change of the binding energy of the Fe $2p_{3/2}$ and $2p_{1/2}$ signals and, thus, the oxidation state of Fe remains close to +2 after the separation. Instead an additional shoulder is found in the spectrum of the recycled LFP at binding energies of $\approx$707.0 eV, which corresponds well to pyrite FeS_2.[41] The presence of pyrite within the recycled LFP might also explain the observed color change after the separation.[45] The P 2p signal of both samples are very similar and confirm the predominant presence of phosphate species PO_4^{3-} of $LiFePO_4$.[46] The S 2p spectrum for recycled LFP confirms again the formation of sulfidic species on the particle surfaces.[38,41,42,47]

**ADVANCED
SCIENCE NEWS**

www.advancedsciencenews.com

**ADVANCED
ENERGY & SUSTAINABILITY
RESEARCH**
Open Access
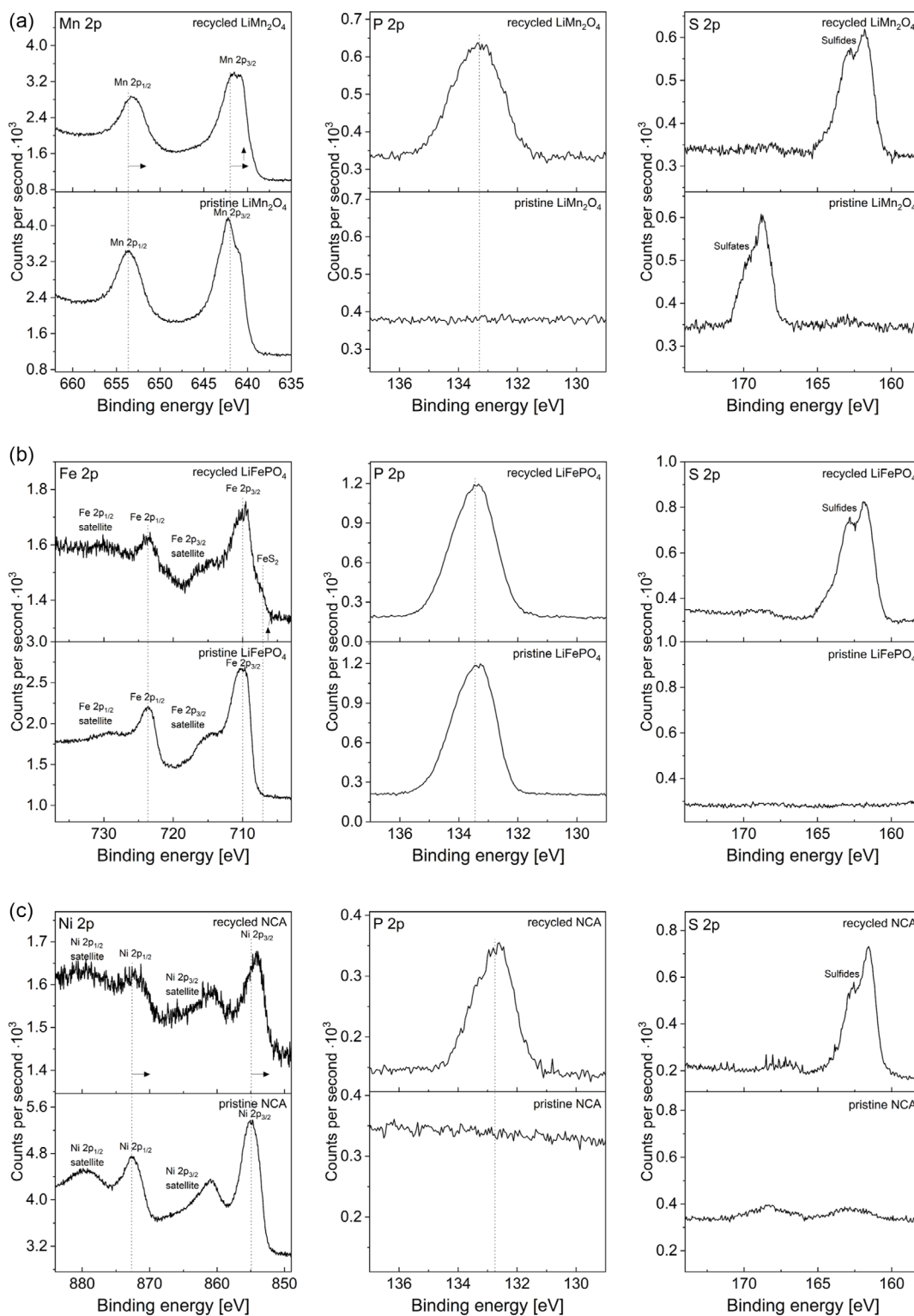
www.advenergysustres.com

Figure 5. Comparison of a) Mn 2p, P 2p, and S 2p XP spectra of pristine and recycled LMO, b) Fe 2p, P 2p, and S 2p XP spectra of pristine and recycled LFP, c) Ni 2p, P 2p, and S 2p XP spectra of pristine and recycled NCA.

For NCA, in accordance with the previous results, the shift of the Ni 2p spectrum toward lower binding energies confirms a decrease of the Ni oxidation state related to the decomposition of the layered oxide and the formation of NiO within the recycled NCA.[48] Compared to the P 2p spectra of recycled LMO and LFP, the spectrum of recycled NCA is slightly shifted toward lower binding energies which implies the presence of a higher fraction of P—S bonds of β-Li_3PS_4 instead of P—$[S]_n$—P and oxygenated phosphorous species. In addition, the S 2p signal has a smaller width indicating lesser P—$[S]_n$—P species. The XPS measurements of NMC811 (Figure S7, Supporting Information) shows similar trends compared to NCA. However, in agreement with the previous findings, the decomposition under formation of NiO is significantly less pronounced. Additionally, significantly fewer P and S are observed.

Finally, the electrochemical behavior of the recycled electrode materials was examined in comparison to the pristine materials.

For this, Li-ion batteries with an organic liquid electrolyte and tape-casted electrodes were assembled and cycled against metallic Li. Currently, the preparation of functional all-solid-state Li-ion batteries remains challenging and many factors can influence the electrochemical performance of such cells complicating the interpretation of results. Thus, to allow for a distinct identification of differences between the pristine and recycled materials tracing back to the dissolution-based separation process, a conventional cell setup was chosen and CV measurements were performed. GCPL measurements were additionally conducted at different C rates (Figure S8, Supporting Information) and the corresponding rate capability was investigated (Figure S9, Supporting Information). In general, the presence of phosphor and/or sulfur-containing species on the particles can be expected to have an influence on the cycling of the recycled materials as also observed in the performed electrochemical measurements.
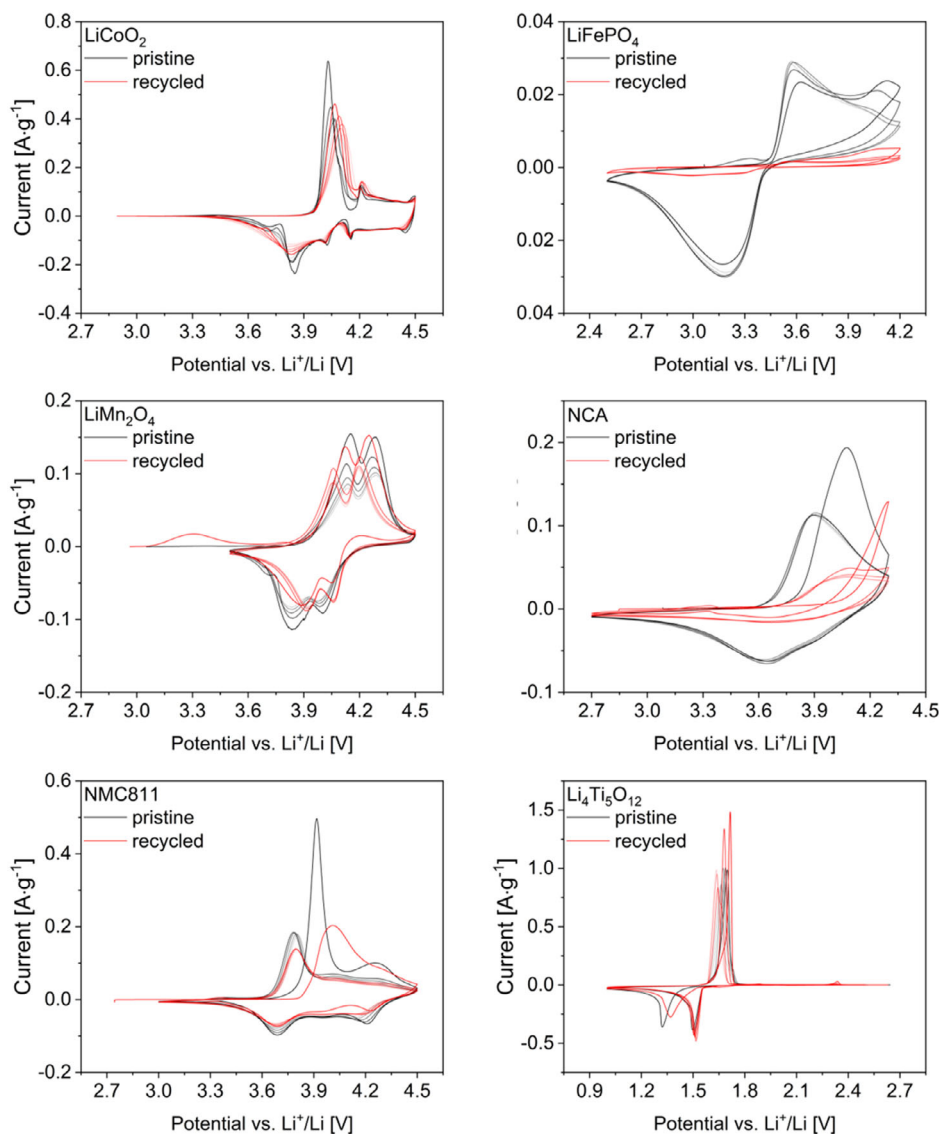

Figure 6. Comparison of CV measurements of pristine and recycled electrode materials.

2300280 (12 of 15)

For LCO and LTO, a good cycling behavior is found for both the pristine and recycled electrode material (**Figure 6**). The cycling performances are comparable to similar electrode materials reported in literature.[33,49] This observation aligns with the found minimal morphological and compositional changes in both the electrode as well as the electrolyte fractions.

Compared to this, pristine and recycled LMO, NMC811, LFP, and NCA show significantly altered charging and discharging curves. In particular, for LFP and NCA, a deterioration of the cycling behavior is observed after the separation process. For LMO and NMC811, the main differences are found between the first cycle of the pristine and recycled electrode materials, whereas the subsequent cycles are fairly similar. Due to the presence of $Li_{1+x}Mn_2O_4$ in the recycled LMO, an additional oxidative peak at $\approx 3.3\,V$ is related to the oxidative delithiation to $LiMn_2O_4$. The limitation of the discharging potential to $>3.5\,V$ does not allow for formation of fully lithiated $Li_2Mn_2O_4$ during the subsequent discharging steps. Instead, only semi-discharged $LiMn_2O_4$ is formed and cycled in the following cycles. The comparison between the pristine and recycled NMC811 reveals a difference between the oxidation peak during the initial charging. While for pristine NMC811, a comparatively sharp peak is found at $\approx 3.9\,V$, a broader peak shifted to $\approx 4.0\,V$ is observed for the recycled NMC811. Nevertheless, starting from the second cycle comparable charging and discharging curves are found for pristine and recycled LMO and NMC811, respectively.

In contrast to this, recycled LFP and NCA show significantly degradation. Though the pristine LFP shows already fairly low redox currents (note that the material was not coated with carbon which is in general required due to the poor electronic conductivity of LFP), even worse behavior is found after the separation. This might be related to the formation of FeS_2 on the particle surfaces as shown by XPS. FeS_2 is known to have a low Li-ion conductivity.[50] For the recycled NCA, a strong decomposition under the formation of large fractions of NiO is observed. Though a thin layer of NiO has been reported to allow for a stabilization of the surface of Ni-rich cathodes, increased formation considerably increases the kinetic barrier for Li-ion diffusion.[26]

4. Conclusions

In this article, it was shown that β-Li_3PS_4 can be separated from TMO electrode materials by dissolution in NMF. Despite the separation results in a recovery of recycled β-Li_3PS_4 and electrode materials with relatively high purity, interactions between the materials during the dissolution process can cause strong changes in functional properties of both components. Interestingly, this behavior is hard to predict and different degradation reactions are observed. Though it can be assumed that the low stability of β-Li_3PS_4 could lead to redox interactions with electrode materials with late transition metals in high oxidation states, the impact on the electrolyte conductivity varies widely in dependence of the electrode material used. In addition, the electrochemical properties of the electrode materials can also change significantly. Overall, lowest changes in terms of functional properties compared to the respective pristine materials were observed for recycled β-Li_3PS_4 separated from LCO and LTO and the corresponding recycled electrode materials.

Due to the observed complexity of the ongoing interactions, the development of highly efficient recycling strategies enabling a closed-loop economy will likely require individual solutions depending on the cell chemistry since circular processes might be intrinsically different for different material combinations.

Supporting Information

Supporting Information is available from the Wiley Online Library or from the author.

Conflict of Interest

The authors declare no conflict of interest.

Author Contributions

K.W., W.E., and O.C. conceived and designed the study. K.W. prepared the samples and performed measurements and analysis. K.W. wrote the manuscript. A.H. performed ICP–MS measurements on the electrolyte materials under the guidance of R.K. K.K. performed XPS measurements on the electrode materials together with U.S. All authors discussed and revised the work.

Data Availability Statement

The data that support the findings of this study are available from the corresponding author upon reasonable request.

[1] a) F. Zheng, M. Kotobuki, S. F. Song, M. O. Lai, L. Lu, *J. Power Sources* **2018**, *389*, 198; b) M. M. Ma, M. H. Zhang, B. T. Jiang, Y. Du, B. C. Hu, C. G. Sun, *Mater. Chem. Front.* **2023**, *7*, 1268; c) X. Zhao, Z. Zhao-Karger, M. Fichtner, X. Shen, *Angew. Chem. Int. Ed. Engl.* **2020**, *59*, 5902; d) D. H. S. Tan, A. Banerjee, Z. Chen, Y. S. Meng, *Nat. Nanotechnol.* **2020**, *15*, 170.

[2] Q. Zhang, D. Cao, Y. Ma, A. Natan, P. Aurora, H. Zhu, *Adv. Mater.* **2019**, *31*, e1901131.

[3] a) Y. Q. He, X. Yuan, G. W. Zhang, H. F. Wang, T. Zhang, W. N. Xie, L. P. Li, *Sci. Total Environ.* **2021**, *766*, 022025; b) M. Velázquez, J. Valio, A. Santasalo, Reuter, G. Serna, *Batteries* **2019**, *5*, 68; c) F. Arshad, L. Li, K. Amin, E. Fan, N. Manurkar, A. Ahmad,

J. Yang, F. Wu, R. Chen, *ACS Sustainable Chem. Eng.* **2020**, *8*, 13527; d) Y. Chen, A. Dou, Y. Zhang, *Front. Mater.* **2021**, *8*, 634667.

[4] a) M. Shahjalal, P. K. Roy, T. Shams, A. Fly, J. I. Chowdhury, M. R. Ahmed, K. Liu, *Energy* **2022**, *241*, 122881; b) X. Wu, G. Ji, J. Wang, G. Zhou, Z. Liang, *Adv. Mater.* **2023**, *35*, e2301540.

[5] X. Wu, J. Ma, J. Wang, X. Zhang, G. Zhou, Z. Liang, *Global Challenge* **2022**, *6*, 2200067.

[6] a) J. X. Wang, J. Ma, K. Jia, Z. Liang, G. J. Ji, Y. Zhao, B. H. Li, G. M. Zhou, H. M. Cheng, *ACS Energy Lett.* **2022**, *7*, 2816; b) K. Jia, J. Wang, Z. Zhuang, Z. Piao, M. Zhang, Z. Liang, G. Ji, J. Ma, H. Ji, W. Yao, G. Zhou, H. M. Cheng, *J. Am. Chem. Soc.* **2023**, *145*, 7288; c) J. X. Wang, K. Jia, J. Ma, Z. Liang, Z. F. Zhuang, Y. Zhao, B. H. Li, G. M. Zhou, H. M. Cheng, *Nat. Sustain.* **2023**, *6*, 797; d) K. Jia, J. Ma, J. Wang, Z. Liang, G. Ji, Z. Piao, R. Gao, Y. Zhu, Z. Zhuang, G. Zhou, H. M. Cheng, *Adv. Mater.* **2023**, *35*, e2208034.

[7] a) M. Jacob, K. Wissel, O. Clemens, *Materials Futures* **2024**, *3*, 012101; b) J. Wu, S. Liu, F. Han, X. Yao, C. Wang, *Adv. Mater.* **2021**, *33*, e2000751.

[8] a) Y. J. Nam, S. J. Cho, D. Y. Oh, J. M. Lim, S. Y. Kim, J. H. Song, Y. G. Lee, S. Y. Lee, Y. S. Jung, *Nano Lett.* **2015**, *15*, 3317; b) K. Lee, S. Kim, J. Park, S. H. Park, A. Coskun, D. S. Jung, W. Cho, J. W. Choi, *J. Electrochem. Soc.* **2017**, *164*, A2075; c) A. Sakuda, K. Kuratani, M. Yamamoto, M. Takahashi, T. Takeuchi, H. Kobayashi, *J. Electrochem. Soc.* **2017**, *164*, A2474; d) M. Yamamoto, Y. Terauchi, A. Sakuda, M. Takahashi, *J. Power Sources* **2018**, *402*, 506; e) M. Yamamoto, Y. Terauchi, A. Sakuda, M. Takahashi, *Sci. Rep.* **2018**, *8*, 1212; f) M. Yamamoto, M. Takahashi, Y. Terauchi, Y. Kobayashi, S. Ikeda, A. Sakuda, *J. Ceram. Soc. Jpn.* **2017**, *125*, 391; g) S. Ito, S. Fujiki, T. Yamada, Y. Aihara, Y. Park, T. Y. Kim, S. W. Baek, J. M. Lee, S. Doo, N. Machida, *J. Power Sources* **2014**, *248*, 943; h) Z. D. Hood, H. Wang, A. S. Pandian, R. Peng, K. D. Gilroy, M. F. Chi, C. D. Liang, Y. N. Xia, *Adv. Energy Mater.* **2018**, *8*, 1800014; i) D. Y. Oh, D. H. Kim, S. H. Jung, J. G. Han, N. S. Choi, Y. S. Jung, *J. Mater. Chem. A* **2017**, *5*, 20771.

[9] L. Azhari, S. Bong, X. Ma, Y. Wang, *Matter* **2020**, *3*, 1845.

[10] D. H. S. Tan, P. Xu, H. Yang, M.-c. Kim, H. Nguyen, E. A. Wu, J.-M. Doux, A. Banerjee, Y. S. Meng, Z. Chen, *MRS Energy Sustain.* **2020**, *7*, E23.

[11] a) S. Yubuchi, M. Uematsu, C. Hotehama, A. Sakuda, A. Hayashi, M. Tatsumisago, *J. Mater. Chem. A* **2019**, *7*, 558; b) L. Zhou, K.-H. Park, X. Sun, F. Lalère, T. Adermann, P. Hartmann, L. F. Nazar, *ACS Energy Lett.* **2018**, *4*, 265; c) S. Yubuchi, M. Uematsu, M. Deguchi, A. Hayashi, M. Tatsumisago, *ACS Appl. Energy Mater.* **2018**, *1*, 3622.

[12] K. Wissel, L. M. Riegger, C. Schneider, A. I. Waidha, T. Famprikis, Y. Ikeda, B. Grabowski, R. E. Dinnebier, B. V. Lotsch, J. Janek, W. Ensinger, O. Clemens, *ACS Appl. Energy Mater.* **2023**, *6*, 7790.

[13] S. K. Sharma, G. Sharma, A. Gaur, A. Arya, F. S. Mirsafi, R. Abolhassani, H. G. Rubahn, J. S. Yu, Y. K. Mishra, *Energy Adv.* **2022**, *1*, 457.

[14] Y. Zhu, X. He, Y. Mo, *ACS Appl. Mater. Interfaces* **2015**, *7*, 23685.

[15] X. Wang, J. Y. Cai, Y. Ren, M. Benamara, X. W. Zhou, Y. Li, Z. H. Chen, H. Zhou, X. H. Xiao, Y. Z. Liu, X. B. Meng, *J. Energy Chem.* **2022**, *69*, 531.

[16] Z. Qiu, Y. Zhang, P. Dong, S. Xia, Y. Yao, *Solid State Ionics* **2017**, *307*, 73.

[17] M. C. Biesinger, *Appl. Surf. Sci.* **2022**, *597*, 153681.

[18] N. Fairley, V. Fernandez, M. Richard-Plouet, C. Guillot-Deudon, J. Walton, E. Smith, D. Flahaut, M. Greiner, M. Biesinger, S. Tougaard, D. Morgan, J. Baltrusaitis, *Appl. Surf. Sci. Adv.* **2021**, *5*, 100112.

[19] D. A. Shirley, *Phys. Rev. B* **1972**, *5*, 4709.

[20] J. F. Moulder, J. Chastain, *Handbook of X-ray Photoelectron Spectroscopy: A Reference Book of Standard Spectra for Identification and Interpretation of XPS Data*, Physical Electronics Division, Perkin-Elmer Corporation, Shelton, CT **1992**.

[21] a) M. Ghidiu, J. Ruhl, S. P. Culver, W. G. Zeier, *J. Mater. Chem. A* **2019**, *7*, 17735; b) K. H. Wujcik, T. A. Pascal, C. D. Pemmaraju, D. Devaux, W. C. Stolte, N. P. Balsara, D. Prendergast, *Adv. Energy Mater.* **2015**, *5*, 1500285; c) K. H. Wujcik, D. R. Wang, A. Raghunathan, M. Drake, T. A. Pascal, D. Prendergast, N. P. Balsara, *J. Phys. Chem. C* **2016**, *120*, 18403.

[22] A. Bartecki, *Rev. Inorg. Chem.* **1992**, *12*, 35.

[23] K. Kaup, L. Zhou, A. Huq, L. F. Nazar, *J. Mater. Chem. A* **2020**, *8*, 12446.

[24] a) C. Dietrich, D. A. Weber, S. Culver, A. Senyshyn, S. J. Sedlmaier, S. Indris, J. Janek, W. G. Zeier, *Inorg. Chem.* **2017**, *56*, 6681; b) H. Yamane, M. Shibata, Y. Shimane, T. Junke, Y. Seino, S. Adams, K. Minami, A. Hayashi, M. Tatsumisago, *Solid State Ionics* **2007**, *178*, 1163; c) C. Dietrich, M. Sadowski, S. Sicolo, D. A. Weber, S. J. Sedlmaier, K. S. Weldert, S. Indris, K. Albe, J. Janek, W. G. Zeier, *Chem. Mater.* **2016**, *28*, 8764.

[25] a) C. J. Lv, Z. G. Li, X. N. Ren, K. X. Li, J. M. Ma, X. C. Duan, *J. Mater. Chem. A* **2021**, *9*, 3995; b) Q. Xie, A. Manthiram, *Chem. Mater.* **2020**, *32*, 7413.

[26] a) J. Li, G. Liang, W. Zheng, S. Zhang, K. Davey, W. K. Pang, Z. Guo, *Nano Mater. Sci.* **2023**, *5*, 404; b) J. Yang, Y. Y. Xia, *J. Electrochem. Soc.* **2016**, *163*, A2665.

[27] a) K. Yamamoto, M. Takahashi, K. Ohara, N. H. H. Phuc, S. Yang, T. Watanabe, T. Uchiyama, A. Sakuda, A. Hayashi, M. Tatsumisago, H. Muto, A. Matsuda, Y. Uchimoto, *ACS Omega* **2020**, *5*, 26287; b) M. Takahashi, S. Yang, K. Yamamoto, K. Ohara, N. H. H. Phuc, T. Watanabe, T. Uchiyama, A. Sakuda, A. Hayashi, M. Tatsumisago, H. Muto, A. Matsuda, Y. Uchimoto, *Solid State Ionics* **2021**, *361*, 115568.

[28] a) Z. Liu, W. Fu, E. A. Payzant, X. Yu, Z. Wu, N. J. Dudney, J. Kiggans, K. Hong, A. J. Rondinone, C. Liang, *J. Am. Chem. Soc.* **2013**, *135*, 975; b) H. Wang, Z. D. Hood, Y. N. Xia, C. D. Liang, *J. Mater. Chem. A* **2016**, *4*, 8091.

[29] M. Calpa, H. Nakajima, S. Mori, Y. Goto, Y. Mizuguchi, C. Moriyoshi, Y. Kuroiwa, N. C. Rosero-Navarro, A. Miura, K. Tadanaga, *Inorg. Chem.* **2021**, *60*, 6964.

[30] a) J. R. Xu, Q. C. Wang, W. L. Yan, L. Q. Chen, H. Li, F. Wu, *Chin. Phys. B* **2022**, *31*, 098203; b) B. R. Shin, Y. J. Nam, D. Y. Oh, D. H. Kim, J. W. Kim, Y. S. Jung, *Electrochim. Acta* **2014**, *146*, 395; c) K. Minami, F. Mizuno, A. Hayashi, M. Tatsumisago, *Solid State Ionics* **2007**, *178*, 837.

[31] R. Kanno, M. Murayama, *J. Electrochem. Soc.* **2001**, *148*, A742.

[32] a) S. S. Zhang, J. Chen, C. S. Wang, *J. Electrochem. Soc.* **2019**, *166*, A487; b) X. Liang, C. Hart, Q. Pang, A. Garsuch, T. Weiss, L. F. Nazar, *Nat Commun* **2015**, *6*, 5682; c) S. H. Akella, S. Taragin, A. Mukherjee, O. Lidor-Shalev, H. Aviv, M. Zysler, D. Sharon, M. Noked, *J. Electrochem. Soc.* **2021**, *168*, 080543.

[33] a) R. Lakshmanan, D. Bhuvaneswari, N. Kalaiselvi, *Met. Mater. Int.* **2012**, *18*, 249; b) L. Li, J. Sui, R. Huang, W. Xiang, W. Qin, *RSC Adv.* **2017**, *7*, 42289; c) K. Chudzik, M. Lis, M. Swietoslawski, M. Bakierska, M. Gajewska, M. Molenda, *J. Power Sources* **2019**, *434*, 226725; d) Y. J. Bi, Y. B. Xu, R. Yi, D. Y. Liu, P. Zuo, J. T. Hu, Q. Y. Li, J. Wu, C. M. Wang, S. Tan, E. Y. Hu, J. N. Li, R. O'Toole, L. Luo, X. G. Hao, S. Venkatachalam, J. Rijssenbeek, J. Xiao, *Energy Storage Mater.* **2023**, *62*, 102947; e) X. Guo, H. F. Xiang, T. P. Zhou, W. H. Li, X. W. Wang, J. X. Zhou, Y. Yu, *Electrochim. Acta* **2013**, *109*, 33.

**ADVANCED
SCIENCE NEWS**

www.advancedsciencenews.com

**ADVANCED
ENERGY & SUSTAINABILITY
RESEARCH**
Open Access

www.advenergysustres.com

[34] T. Pussacq, H. Kabbour, S. Coils, H. Vezin, S. Saitzek, O. Gardoll, C. Tasse, H. Kageyama, C. L. Robert, O. Mentré, *Chem. Mater.* **2017**, *29*, 1047.

[35] a) Q. Wu, J. Xu, Q. Zhuang, S. Sun, *Solid State Ionics* **2006**, *177*, 1483; b) J. W. Murray, J. G. Dillard, R. Giovanoli, H. Moers, W. Stumm, *Geochim. Cosmochim. Acta* **1985**, *49*, 463; c) R. P. Gupta, S. K. Sen, *Phys. Rev. B* **1974**, *10*, 71.

[36] K. M. Shaju, G. V. S. Rao, B. V. R. Chowdari, *Solid State Ionics* **2002**, *152*, 69.

[37] B. R. Strohmeier, D. M. Hercules, *J. Phys. Chem.* **2002**, *88*, 4922.

[38] a) A. Kato, H. Kowada, M. Deguchi, C. Hotehama, A. Hayashi, M. Tatsumisago, *Solid State Ionics* **2018**, *322*, 1; b) S. Wenzel, S. J. Sedlmaier, C. Dietrich, W. G. Zeier, J. Janek, *Solid State Ionics* **2018**, *318*, 102; c) K. N. Wood, K. X. Steirer, S. E. Hafner, C. Ban, S. Santhanagopalan, S. H. Lee, G. Teeter, *Nat. Commun.* **2018**, *9*, 2490.

[39] a) Y. Ma, J. H. Teo, F. Walther, Y. J. Ma, R. Z. Zhang, A. Mazilkin, Y. S. Tang, D. Goonetilleke, J. Janek, M. Bianchini, T. Brezesinski, *Adv. Funct. Mater.* **2022**, *32*, 2111829; b) J. H. Teo, F. Strauss, F. Walther, Y. Ma, S. Payandeh, T. Scherer, M. Bianchini, J. Janek, T. Brezesinski, *Mater. Futures* **2022**, *1*, 015102.

[40] a) J. P. R. Vissers, C. K. Groot, E. M. Vanoers, V. H. J. Debeer, R. Prins, *Bull. Soc. Chim. Belg.* **1984**, *93*, 813; b) H. F. Franzen, M. X. Umana, J. R. Mccreary, R. J. Thorn, *J. Solid State Chem.* **1976**, *18*, 363.

[41] H. van der Heide, R. Hemmel, C. F. van Bruggen, C. Haas, *J. Solid State Chem.* **1980**, *33*, 17.

[42] Y. Wang, T. Matsuyama, M. Deguchi, A. Hayashi, A. Nakao, M. Tatsumisago, *J. Ceram. Soc. Jpn.* **2016**, *124*, 597.

[43] R. Koerver, F. Walther, I. Aygün, J. Sann, C. Dietrich, W. G. Zeier, J. Janek, *J. Mater. Chem. A* **2017**, *5*, 22750.

[44] X. R. Yu, F. Liu, Z. Y. Wang, Y. Chen, *J. Electron. Spectrosc. Relat. Phenom.* **1990**, *50*, 159.

[45] K. Xi, D. He, C. Harris, Y. Wang, C. Lai, H. Li, P. R. Coxon, S. Ding, C. Wang, R. V. Kumar, *Adv. Sci.* **2019**, *6*, 1800815.

[46] a) R. Liu, J. Chen, Z. Li, Q. Ding, X. An, Y. Pan, Z. Zheng, M. Yang, D. Fu, *Materials* **2018**, *11*, 2251; b) J. W. Zhang, H. X. Yu, X. K. Zhang, M. T. Xia, X. Q. Zhang, L. Y. Zhang, M. Shui, Y. H. Cui, J. Shu, *Ionics* **2021**, *27*, 31.

[47] H. Binder, *Z. Naturforsch.* **1973**, *28b*, 255.

[48] a) P. Xiao, W. Li, S. Chen, G. Li, Z. Dai, M. Feng, X. Chen, W. Yang, *ACS Appl. Mater. Interfaces* **2022**, *14*, 31851; b) W. Xiao, Y. Nie, C. Miao, J. Wang, Y. Tan, M. Wen, *J. Colloid Interface Sci.* **2022**, *607*, 1071.

[49] a) G. J. Wang, Q. T. Qu, B. Wang, Y. Shi, S. Tian, Y. P. Wu, R. Holze, *Electrochim. Acta* **2009**, *54*, 1199; b) Y. Guo, Y. Wei, H. Li, T. Zhai, *Small* **2017**, *13*, 1701649.

[50] J. H. Lu, F. Lian, L. L. Guan, Y. X. Zhang, F. Ding, *J. Mater. Chem. A* **2019**, *7*, 991.